# Quantitation of Ion Abundances in Fourier Transform Ion Cyclotron Resonance Mass Spectrometry

Kevin L. Goodner,* K. Eric Milgram,† Kathryn R. Williams, Clifford H. Watson,‡ and John R. Eyler
Department of Chemistry, University of Florida, Gainesville, Florida, USA

To improve the analytical usefulness of Fourier transform ion cyclotron resonance mass spectrometry (FTICR-MS), an extensive survey of various methods for quantitation of peak magnitudes has been undertaken using a series of simulated transient response signals with varying signal-to-noise ratio. Both peak height (five methods) and peak area (four methods) were explored for a range of conditions to determine the optimum methodology for quantitation. Variables included dataset size, apodization function, damping constant, and zero filling. Based on the results obtained, recommended procedures for optimal quantitation include: apodization using a function appropriate for the peak height ratios observed in the spectrum (i.e., Hanning for ratios of about 1:10, three-term Blackman-Harris for ratios of ~1:100, or Kaiser-Bessel for ratios of ~1:1000); zero filling until the peaks of interest are represented by 10–15 points (generally obtained with one order of zero filling); and use of the polynomial $y = (ax^2 + bx + c)^n$ and the three data points of highest intensity of the peak to locate the peak maximum, $Y_{max} = (-b^2/4a + c)^n$. In this peak fitting procedure, which we have termed the "Comisarow method," $n$ is 5.5, 9.5, and 12.5 for the Hanning, three-term Blackman-Harris, and Kaiser-Bessel apodization functions, respectively. Accuracy of quantitation using an optimal peak height determination is about equal to that for peak area measurements. These recommendations were found to be valid when tested with real FTICR-MS spectra of xenon isotopes. (J Am Soc Mass Spectrom 1998, 9, 1204–1212) © 1998 American Society for Mass Spectrometry

The technique of Fourier transform ion cyclotron resonance mass spectrometry (FTICR-MS) has been used quite successfully to obtain data for qualitative studies. These have included structure elucidation [1, 2], determination of fragmentation pathways [3, 4] and reaction mechanisms [5, 6], and exact mass measurements [7, 8]. However, *quantitative* analysis using FTICR has received considerably less attention, even though there are many applications that require relative and absolute ion abundances of the highest possible accuracy and precision. An obvious need is the determination of unknown concentrations using appropriate calibration curves. Another example is the determination of ion/neutral binding energies [9], which requires high-accuracy ion abundance measurements. Reaction rate coefficient and equilibrium constant measurements are also affected by the uncertainty in measured peak magnitudes. It is thus imperative that the determination of FTICR-MS ion abundances be optimized for maximum accuracy and precision. The present work reports an investigation of various factors affecting FTICR-MS peak measurements to determine the method that gives highest quality data with minimal increase in analysis time.

Various researchers have examined the variables involved in analyzing FTICR-MS signals with the primary goal of achieving the highest possible mass accuracy [10–21]. Their investigations included evaluation of apodization functions [10–16], zero filling [17], and various interpolation/fitting functions [18–21] to give a more accurate assessment of the exact frequency (and thus mass) of peak maxima. These improvements are very important for qualitative analyses, but for quantitative analyses the mass of the analyte is often known and information on the relative or absolute ion abundance is desired instead.

Liang and Marshall reported a method for determining precise relative ion abundances using a least-squares fit of the peak to a Lorentzian lineshape [18]. The results were impressive, but with two major disadvantages. The method is stated to be most appropriate when there is no peak overlap, and the data fitted in the

Address reprint requests to Dr. John R. Eyler, Department of Chemistry, P.O. Box 117200, University of Florida, Gainesville, FL 32611-7200. E-mail: eyler@chem.ufl.edu

* Present address: University of Florida, Citrus Research and Education Center, 700 Experiment Station Rd., Lake Alfred, FL 33850.

† Present address: U.S. Centers for Disease Control and Prevention, Bldg. 17 Mailstop F-17, 4770 Buford Highway NE, Atlanta, GA 30341-3724.

‡ Present address: U.S. Centers for Disease Control and Prevention, Bldg. 17 Mailstop F-19, 4770 Buford Highway NE, Atlanta, GA 30341-3724.


1044-0305/98/$19.00
PII S1044-0305(98)00090-7

Received September 4, 1997
Revised June 29, 1998
Accepted June 29, 1998

paper were not apodized. However, apodization of the time-domain response signal is commonly used in FTICR mass spectrometry to minimize peak side lobes and to observe small peaks that may be obscured in the "ringing" from adjacent larger peaks. Because many applications require quantitation of closely spaced peaks, whose side lobes could overlap in the absence of apodization, the Liang and Marshall technique is limited to relatively isolated peaks.

This report builds on previous studies by applying similar methodologies to the determination of accurate peak magnitudes. Several methods for measuring both peak height and peak area are examined and evaluated using simulated datasets having different numbers of data points, signal-to-noise ratios, and damping constants. The resulting optimum methodology is tested with some experimental data obtained from FTICR measurements of xenon isotopes.

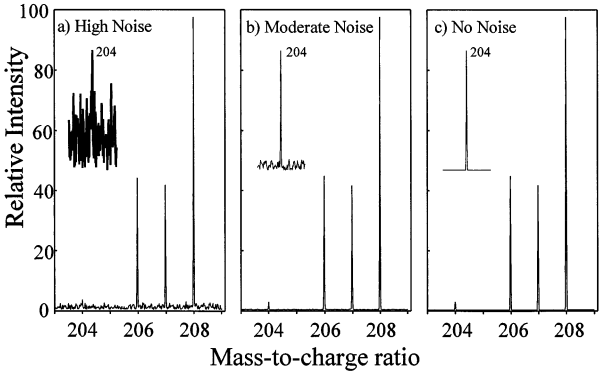


**Figure 1.** Examples of the three types of simulated spectra used in this study with a 32k dataset, three-term Blackman-Harris apodization, and no zero filling: (a) high-noise spectrum, (b) moderate-noise spectrum, (c) no-noise spectrum. The insets show a ~15× expansion of the relative magnitude in the region around $m/z$ 204 to better indicate the signal-to-noise ratio.

## Methodology

To make accurate comparisons between quantitation methods, it is essential to have exact knowledge of the true peak magnitudes. For this reason, the present study was based on the analysis of simulated FTICR transient responses. All signal generation and treatment were performed using a 80486DX2-80MHz computer and the Windows©-based analysis package, WINICR, written in this laboratory [22]. Double-precision floating point variables were used for all calculations.

Transient response signals representative of the desired abundances were generated by adding a series of cosine functions with appropriate amplitude factors and with frequencies corresponding to the ion masses of interest. Eight ion masses were chosen for the simulated signals: singly charged lead ions ($Pb^+$) at $m/z$ 204, 206, 207, and 208, and the corresponding doubly charged lead ions ($Pb^{+2}$) at $m/z$ 102, 103, 103.5, and 104. To mimic the naturally occurring abundances of these isotopes [23], relative amplitudes of 1.4, 24.1, 22.1, and 52.4 were assigned to the cosine signals for a mass-to-charge ratio equal to 204, 206, 207, and 208, respectively, and correspondingly for $m/z$ 102, 103, 103.5, and 104. Transient response signals were generated for four dataset sizes: 16k, 32k, 64k, and 128k data points.

For each of the four dataset sizes, transient response signals with three different noise levels were generated by adding random numbers in the ranges −15 to 15, −1.5 to 1.5, and 0, respectively, to the transient response signal, in which the extrema ranged from +200 to −200 prior to noise addition. Figure 1 illustrates the effect of these three noise levels on the transformed data. The left spectrum (Figure 1a), which corresponds to addition of random numbers between −15 and +15 to each point of the transient response signal, is labeled "high noise," and represents a signal-to-noise ratio (S/N) typical of spectra obtained by transformation of a single transient. The middle spectrum (Figure 1b), with addition of a random number from −1.5 to +1.5 to each point of the transient, is labeled as "moderate noise." Its S/N is ten times that of the left spectrum, typical of what would be seen if 100 transients were averaged (S/N $\propto n^{1/2}$, where $n$ is the number of transients [24]). The right spectrum (Figure 1c) is labeled "no noise," because no noise was added to the transient response signal. This corresponds to averaging an infinite number of scans prior to transformation. These three noise levels were chosen to represent worst, normal, and ideal cases, with the moderate noise level representative of typical FTICR situations. Because of the high noise level in the "single-scan" spectrum, the smallest peak (1.4% abundance for $m/z$ 102 and 204) was generally not discernible from the noise and was not used for quantitation. Although theoretically a more correct assessment of the effect of noise on data analysis could be obtained by using Gaussian-distributed random noise, the approach used here adds noise to the time domain transients in a way that adequately permits the analysis of spectra of differing signal-to-noise levels.

In real FTICR-MS experiments, the observed signal is damped by collisions of the ions with neutral gas molecules. To investigate this effect, additional damped transient response signals were generated. The simulated data sets were artificially damped by multiplication by an exponential function of the form

$$e^{(-k/\tau)}, \qquad 1 \le k \le T \tag{1}$$

where $k$ is the data index number, $\tau$ is the damping constant, and $T$ is the total number of data points. A value of $2^{15}$(= 32k) was used for $\tau$, resulting in attenuation of the final data point of the transient by a factor of $e(-0.5)$, $e(-1)$, $e(-2)$, and $e(-4)$ for the 16k, 32k, 64k, and 128k data sets, respectively. Equation 1 is the most common model currently in use for FTICR damping. New studies have suggested that this model is appropriate for low-mass ions, such as the ones exam-

**Table 1.** Apodization functions

| Name | Analytical form, $0 < t < T$[a] |
|---|---|
| Three-term Blackman-Harris | $0.42323 - 0.49755 \cos(2\pi t/T) + 0.07922 \cos(4\pi t/T)$ |
| Kaiser-Bessel | $I_0(3.5\pi\{1.0 - [(2t - T)/T]^2\}^{0.5})/I_0(3.5\pi)$[b] |
| Hamming | $0.54 - 0.46 \cos(2\pi t/T)$ |
| Hanning | $\sin^2(\pi t/T)$ |

[a] $T$ is the total acquisition time, and the transient response signal is collected over times $t$ from 0 to $T$.
[b] $I_0(x)$ is the zero-order modified Bessel function.

ined in this study, but for high-mass molecules, such as biopolymers, another model would be more accurate [25].

The combination of four dataset sizes with three noise levels and two types of signal damping gave 24 simulated transient response signals. Once these were generated, the effect of applying various apodization functions was investigated. Apodization involves multiplying the time-domain transient by a function in order to minimize side lobes or "feet" in the frequency domain spectrum [26]. These side lobes arise from the abrupt truncation of the transient response signal at the beginning and end of data acquisition in the time domain. The apodization functions used in this study minimize this problem by forcing the beginning and ending portions of the transient response signal to approach zero monotonically [20].

Several of the most commonly applied FTICR apodization functions were studied, including the Hamming, Hanning, three-term Blackman-Harris, and the Kaiser-Bessel functions. These functions have varying characteristics, which have been studied previously [10–15]. The optimal function for a particular application depends on the relative magnitudes of the peaks of interest [10, 11]. The Hamming or Hanning function is recommended for relative ion abundance ratios of about 1:10, the three-term Blackman-Harris for ~1:100 ratios, and the Kaiser-Bessel for ~1:1000 ratios. The mathematical forms of the individual functions are shown in Table 1. The study was restricted to these four apodization functions, because they are the most common functions used for routine analysis, and because a previous investigation [21] of the most successful method for quantitating peak positions concentrated on these four apodization functions.

Various degrees of zero filling were investigated to assess the effect on quantification. Zero filling doubles the number of points to be transformed by adding zeros to the end of the transient signal, effectively interpolating points in the frequency (mass) spectrum after Fourier transformation. This increases the number of points defining a peak, thus decreasing the error in peak abundance determination. Investigations using no zero filling, and one, two, and three orders of zero filling were undertaken. The transient response signal for each order of zero filling was one, two, four, or eight times the size of the original transient, and, as a result, progressively longer processing times were required for the Fourier transformation. Thus, a total of 16 pretransform manipulations (four apodization functions and four different orders of zero filling) were applied to each transient response signal. Given the 24 simulated transient response signals, this resulted in a total of 384 transformed spectra, each with eight peaks (except for the high-noise case, where only six were used), for a total of 2816 peaks evaluated per quantitation method (peak height and peak area) in this investigation.

Ion abundances were determined from measurements of both peak heights and peak areas taken from magnitude-mode spectra. Peak overlap can be problematic for closely spaced peaks in magnitude-mode spectra because overlapped peak values do not simply add due to partial cancellation of their dispersion-mode components. However, inspection of Figure 1 reveals that the simulated peaks in this analysis are quite well separated.

Five methods of determining peak heights were evaluated. The apex method utilized the maximum data point as the height of the peak. Although this is a straightforward and simple approach, the measured value is never the true peak height, because the true "analog" maximum usually falls between data points [21]. The other methods involved interpolating the peak maximum by fitting the three data points of highest magnitude to various functions, all described by the equation

$$Y = (aX^2 + bX + c)^n \tag{2}$$

where $n$ depends on the type of interpolation, $X$ is the mass-to-charge ratio, and $Y$ is the signal magnitude. For this study, parabolic ($n = 1$), Lorentzian ($n = -1$), magnitude-Lorentzian ($n = -0.5$), and what will be termed the Comisarow method ($n > 1$) fitting functions were examined. The Comisarow method is based on optimized values of $n$ for the various apodization functions [21]: 5.5 for Hanning apodization, 6.6 for Hamming apodization, 9.5 for three-term Blackman-Harris apodization, and 12.5 for Kaiser-Bessel apodization.

To determine the maximum value of a peak, eq 2 was differentiated, and the position of the maximum was subsequently found by setting the derivative equal to zero and solving for $X$:

$$0 = n(aX^2 + bX + c)^{n-1}(2aX + b) \tag{3}$$

In eq 3, $n$ must be either 1, −1, 0.5, 5.5, 6.6, 9.5, or 12.5, depending on the fitting function. The second term, $(aX^2 + bX + c)^{n-1}$, is the peak maximum raised to a power and cannot be zero. Thus, the term $(2aX + b)$ can be set equal to zero to give

$$X_{max} = -b/2a \tag{4}$$

Substituting this expression for $X_{max}$ into eq 2 gives

$$Y_{max} = [a(-b/2a)^2 + b(-b/2a) + c]^n$$
$$= (-b^2/4a + c)^n. \tag{5}$$

To determine the value of $Y_{max}$, three simultaneous equations containing $a$, $b$, and $c$ were obtained using eq 2 for the three data points—$(X_1, Y_1)$, $(X_2, Y_2)$, and $(X_3, Y_3)$—closest to the top of the peak. These three equations were manipulated into matrix form:

$$\begin{bmatrix} X_1^2 & X_1 & 1 \\ X_2^2 & X_2 & 1 \\ X_3^2 & X_3 & 1 \end{bmatrix} \begin{bmatrix} a \\ b \\ c \end{bmatrix} = \begin{bmatrix} Y_1^{1/n} \\ Y_2^{1/n} \\ Y_3^{1/n} \end{bmatrix} \tag{6}$$

The values of $a$, $b$, and $c$ were obtained by inverting the $3 \times 3$ matrix and multiplying both sides of the equation by the inverse matrix to yield a $3 \times 1$ matrix of the coefficients [27]. These operations are accomplished very quickly (typically within 1 ms) on modern computers. After $a$, $b$, and $c$ were evaluated, they were substituted into eq 5 to obtain $Y_{max}$.

Peak area was also studied as a measure of ion abundance. It is known that in the mass domain the full width at half maximum (FWHM) of a FTICR peak increases with increasing mass [28]. However, peak widths are constant in the frequency domain if the detected ions have the same postexcitation kinetic energy and if collisional broadening processes are essentially independent of mass, as expected for stable isotopes of the same element. Thus, frequency-domain areas are viable measures of peak magnitudes and were used for the determinations in this study. The areas were calculated by four procedures, referred to as the trapezoidal, extended trapezoidal, triangle, and integrated Comisarow methods.

For the two trapezoidal methods, the initial and final points of the peak had to be identified. This was accomplished by systematically inspecting all points starting with the peak maximum and proceeding in both directions. The first data point of higher magnitude than the preceding one was taken as the start (or end) of the peak, assuming that either another peak, a side lobe, or noise was causing an increase in magnitude. The triangle method does not require such a determination, and the requirements of the integrated Comisarow method are discussed below.

The trapezoidal area was obtained by summing the frequency difference between two successive data points ($\Delta X$) multiplied by the average peak height ($\bar{Y}$) between the two points,

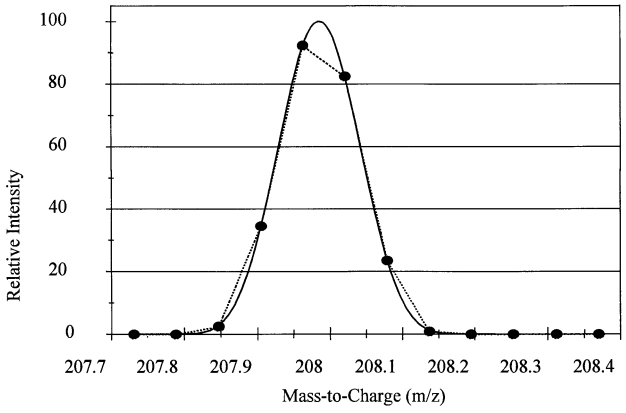


**Figure 2.** Peak fitting by the Comisarow method for $^{208}Pb^{+1}$ using a simulated 32k dataset, no noise, three-term Blackman-Harris apodization function, and no zero filling. The dotted line merely connects the points that were fitted and indicates the peak shape that would be obtained if no fitting were done. The solid line was obtained by using the appropriate Comisarow fitting function (see text) to fit the three points of highest magnitude on the peak.

$$A = \sum_{i=\text{start}}^{i=\text{end}-1} \Delta X_i \times \bar{Y}_i$$
$$= \sum_{i=\text{start}}^{i=\text{end}-1} (X_{i+1} - X_i) \times \frac{1}{2} \times (Y_{i+1} + Y_i) \tag{7}$$

where $X_i$ is the value of the $i$th frequency data point, $Y_i$ is the corresponding magnitude, and start and end values were determined as described above.

Because the true maximum of the peak is not usually the data point of highest magnitude, some of the total peak area is omitted when using the usual trapezoidal method. Therefore, an extended trapezoidal method was developed to include the true peak maximum by using the simple trapezoidal area plus the triangular area with vertices at the Comisarow interpolated maximum (calculated according to eqs 5 and 6) and the two adjacent data points.

The peak shape can also be approximated by an isosceles triangle whose area is equal to the Comisarow interpolated maximum multiplied by the FWHM. To determine the frequency ($X$) values for the FWHM evaluation, the peak height was divided by two, and on each side of the peak the two $X$'s with heights spanning this half-maximum value were found. The $X$ values corresponding to the exact half-maximum were determined by interpolation, and their difference was used as the FWHM.

The final method for estimating peak area was integration of the appropriate Comisarow fitting function [21]. This approach is justified because, as shown in Figure 2, the functions described by Comisarow are able to fit the entire peak, even though only the three data

points nearest the top of the peak are used to determine the constants $a$, $b$, and $c$ in eq 2. The first step in this procedure is determination of the integration limits. First, the FWHM was determined by the procedure described in the previous paragraph. The peak start was located by subtracting the FWHM from the $X$ value at the peak center and subsequently moving back toward the center until $(aX^2+bX+c)$ was positive, using the $a$, $b$, and $c$ values obtained above. The peak end was determined in a similar manner. The peak area is given by

$$A = \int_{X_{\text{start}}}^{X_{\text{end}}} (aX^2 + bX + c)^n \, dx \tag{8}$$

The integral was evaluated from

$$\int \mathbb{R}^z \sqrt{\mathbb{R}} \, dx = \frac{(2z+2)!}{[(z+1)!]^2 (4k)^{z+1}} \cdot \left( \frac{k(2ax+b)\sqrt{\mathbb{R}}}{a} \sum_{r=0}^{z} \frac{r!(r+1)!(4k\mathbb{R})^r}{(2r+2)!} + \int \frac{dx}{\sqrt{\mathbb{R}}} \right) \tag{9}$$

and

$$\int \frac{dx}{\sqrt{\mathbb{R}}} = \begin{cases} \dfrac{1}{\sqrt{a}} \sinh^{-1} \dfrac{2ax+b}{\sqrt{q}} & (a > 0) \\ -\dfrac{1}{\sqrt{-a}} \sin^{-1} \dfrac{2ax+b}{\sqrt{-q}} & (a < 0) \end{cases} \tag{10}$$

where $\mathbb{R} = (aX^2+bX+c)$, $z = n - 0.5$, $q = 4ac - b^2$, and $k = 4c/q$ [23]. To facilitate use of this solution for all four apodization functions, the $n$ for the Hamming apodization was adjusted slightly from 6.6 to 6.5.

For all analyses the accuracy was expressed as the average magnitude of the percent error (APE), given by

$$\text{APE} = \frac{1}{N} \sum_{i=1}^{N} \frac{|A_i - A_t|}{A_t} \times 100\% \tag{11}$$

where $N$ is the number of measurements, $A_i$ is the ion abundance determined for the $i$th measurement, and $A_t$ is the "true" value of the ion abundance, given by the relative amplitude assigned to the cosine function used in the simulation of transient response signals.

## Results and Discussion

### *Quantitation Based on Peak Height*

A summary of the average magnitude of the percent error for quantitation by peak height measurement is shown in Figure 3, which is a bar graph of APEs for various combinations of noise level, zero-filling order, and peak height evaluation method. Each bar was calculated from 48 measured versus "true" comparisons for the high-noise case (six peaks in spectra from transient response signals of four different lengths, for both damped and undamped cases) and 64 comparisons for the moderate-noise and no-noise cases (eight peaks in spectra from transient response signals of four different lengths, for both damped and undamped cases). A Hanning apodization function was used for all data shown in this figure. Results for other apodization functions are discussed below.

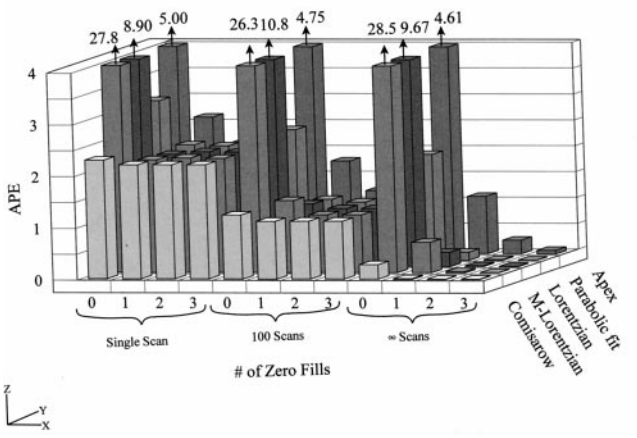


**Figure 3.** Bar graph showing the APE (eq 11) for simulated datasets using peak height as a method for quantitation of ion abundances for various fitting functions, noise levels, and orders of zero filling. The arrows on some bars indicate that they are offscale and have the value above the arrow.

As expected, there is a marked decrease in the average magnitude of the percent error as the noise level is decreased. The lowest APE is about 2.2 for the high-noise set, 1.2 for the moderate-noise set, and 0.01 for the no-noise set. As the number of scans increases, the noise decreases, resulting in less uncertainty in the peak height measurements. Thus, peak quantitation requires a tradeoff between the desired accuracy level versus the additional time required to make repetitive measurements. An increase in the signal-to-noise ratio by a factor of 10 requires a 100-fold increase in the number of transients.

The accuracy also increases with the level of zero filling because of the improved peak definition with a greater number of points (in this example, 6, 11, 22, and 45 points for zero, one, two, and three orders of zero filling, respectively). The improvement is most significant for the first order of zero filling. As shown in Figure 3, there is a sharp reduction in APE for all noise levels and all peak height evaluation methods with a change from no zero filling to one filling order. Only slight improvements are seen with two and three orders. This is the expected result, because the first zero filling effectively combines the information contained in the real and imaginary parts of the Fourier transform

[29], while subsequent orders of zero filling do not contribute any information. Thus, these results indicate that one zero filling is optimum, corresponding in this case to about 10–15 points per peak. Although higher orders of zero filling give slightly better accuracy, the time required for Fourier transformation increases with each order.

Finally, examination of Figure 3 indicates that the Comisarow method gives the lowest APE for the conditions used in this study, and this is especially true when there is no zero filling. As the number of points spanning a peak increases, other methods become comparable to the one based on Comisarow's equation. However, with only one order of zero filling, the Comisarow method performs as well as any method at any zero-fill level. The Comisarow method is also relatively insensitive to zero-fill order compared to the other methods; the APE for two orders of zero filling is 0.997 of that for one order, and the APE for three orders of zero filling is 0.9999 of that for two orders. Thus, in this study the Comisarow method was either statistically the same as or superior to every other method of peak height determination. This result is to be expected, because the Comisarow fitting functions have been shown [21] to be the best for determining the center position of the peak along the frequency (or mass) axis, and thus should be best for determining the peak magnitude at the true peak frequency. The Lorentzian and magnitude Lorentzian methods do not perform as well, because they are intended for use with unapodized spectra. They have been included for completeness and in order to test their applicability to apodized spectra.

The data represented in Figure 3 were obtained using the Hanning apodization function, but the Hamming, three-term Blackman-Harris, and Kaiser-Bessel apodization functions all produced results with trends similar to those shown in Figure 3. The Hanning function was used for Figure 3 because the other apodization functions did not provide APE's quite as low. For example, using the Comisarow method and one order of zero filling, the three-term Blackman-Harris and Kaiser-Bessel functions yielded APE's greater by factors of 1.04 and 1.06 compared to the APE obtained using Hanning apodization. This is to be expected because the relative magnitudes of the measured peaks in this study are approximately 1:2, 1:2, and 1:37. As stated earlier, the Hanning apodization is recommended for peak magnitude ratios of 1:10, while the optimum ratio range is 1:100 and 1:1000 for the three-term Blackman-Harris and the Kaiser-Bessel functions, respectively. Because the magnitude ratio in this study was closest to 1:10, the Hanning apodization provided the best results, with the three-term Blackman-Harris apodization being the next best. Finally, the Hamming function, with APE's larger than those shown in Figure 3 by as much as a factor of 1.40, is clearly a poor choice. This function leaves large side lobes that interfere with peak height determination for closely spaced peaks, especially the $Pb^{+2}$ peaks at 103, 103.5, and 104 $m/z$.

**Table 2.** Effect of dataset size and signal damping on average magnitude of the percent error (APE)

| Signal damping | Dataset size | APE |
|---|---|---|
| Quantitation by peak height[a] | | |
| Undamped | 16k | $1.6_2$ |
| | 32k | $1.2_8$ |
| | 64k | $1.2_2$ |
| | 128k | $0.3_8$ |
| Damped | 16k | $0.2_4$ |
| | 32k | $1.3_2$ |
| | 64k | $1.7_5$ |
| | 128k | $1.1_1$ |
| Quantitation by peak area[b] | | |
| Undamped | 16k | 1.9/1.9 |
| | 32k | 2.0/2.1 |
| | 64k | 1.8/1.9 |
| | 128k | $0.2_9/0.3_4$ |
| Damped | 16k | $0.3_4/0.5_7$ |
| | 32k | 1.1/1.2 |
| | 64k | 2.2/2.6 |
| | 128k | 1.3/1.4 |

[a]Hanning apodization, moderate-noise level, one order of zero filling, Comisarow method.
[b]Hanning apodization, moderate-noise level, one order of zero filling, Comisarow/triangle method.

Because the most accurate results were obtained when using Hanning apodization, one order of zero filling, and the Comisarow method for peak height determination, these parameters were used to investigate the effects of dataset size and exponential signal damping. Results of these investigations are summarized in Table 2. For undamped transients, the APE decreases monotonically with increasing dataset size. This is expected, because, as the number of data points in an undamped transient increases, the signal-to-noise ratio of the transformed spectrum increases, and therefore the three points used in the interpolation have a smaller fraction of noise interfering with accurate determinations. Interpretation of the data for the damped transients is somewhat less straightforward, because both the dataset size and the $T/\tau$ value in eq 1 are changing. Previous studies [19–21] have shown that the interpolation accuracy decreases with increasing $T/\tau$. This explains the general upward trend in APE between datasets of 16k and 64k points. However, the present results indicate that the increased signal to noise, with the resulting increased accuracy of the interpolations, overrides the increased error from greater $T/\tau$ ratios for the larger datasets. These results are in agreement with earlier theoretical noise studies that show the same trend in maxima for damped samples [30].

## *Quantitation Based on Peak Area*

The bar graph for quantitation results based on peak areas is shown in Figure 4. As in Figure 3, a Hanning

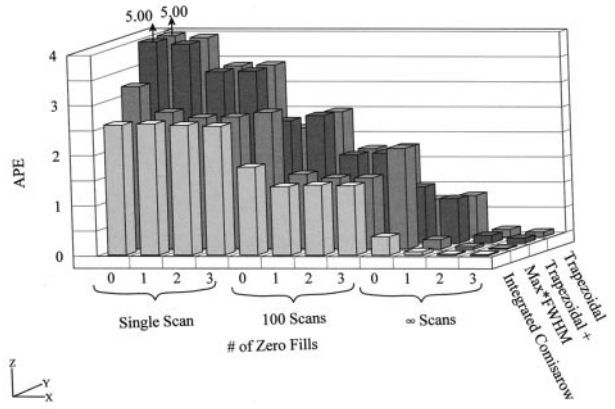


**Figure 4.** Bar graph showing the APE (eq 11) for simulated datasets using peak area as a method for quantitation of ion abundances for various fitting functions, noise levels, and orders of zero filling. The arrows on some bars indicate that they are offscale and have the value above the arrow.

apodization function was used for all data shown. Given that the triangle and integrated Comisarow methods use the peak height as one factor in the area determination, similar quantitation results for the two methods are expected, especially since peak areas and interpolated peak heights are both evaluated from the three data points of highest magnitude. The trapezoidal methods include more points, although the largest contribution is still made by the three data points of highest magnitude.

As with peak height, a decrease in the noise level results in improved accuracy. Considering the areas obtained by the integrated Comisarow method, the APE's decrease from ~2.6% for the high-noise data to ~1.6% for the moderate-noise data to ~0.4% for transients generated with no noise. These APE's are all slightly higher than those obtained using the Comisarow interpolated peak height for quantitation, probably because of uncertainties in locating the peak start and end for use in eq 8. The data in Figure 4 also indicate that one order of zero filling gives the best compromise of quantitation accuracy and transformation time.

Perhaps the most significant features in Figure 4 are the APE trends for the peak area evaluation methods. Considering first the two trapezoidal methods, it is clear that they give almost identical results. The triangle and integrated Comisarow methods yield similar results for high- and moderate-noise cases, except without zero filling, for which the integrated Comisarow method is considerably better at all noise levels. As noted above, the noise level in typical FTICR-MS experiments is similar to that in the moderate-noise spectra. Thus, the results shown in Figure 4 suggest that the integrated Comisarow method is superior for calculating peak areas under most conditions.

As is the case with peak heights, the Hanning apodization function gives the lowest APE's for peak area determination, with APE's from the three-term Blackman-Harris, Kaiser-Bessel, and Hamming apodizations higher by factors of 1.015, 1.019, and 1.616, respectively, when using the integrated Comisarow approach with one order of zero filling. It is apparent that the Hamming apodization function is not desirable for these methods of quantitation, and that one of the other three apodization functions should be used, depending on the relative peak heights in the spectrum [11].

The effects of dataset size and signal damping (Table 2) are similar to those for peak height measurements. Except for the anomalous initial point, there is a general decrease in APE for the undamped signal due to signal-to-noise improvement. The APE's from damped transients initially increase and then decrease because of the competing factors of increasing $T/\tau$, which leads to greater error, and increasing dataset size, which improves the signal-to-noise ratio and decreases the error.

### *Systematic Errors*

As shown in eq 11, the APE is calculated using the magnitude of the error for each measurement without regard to direction. It is also important to consider whether certain combinations of parameters yield systematically high or low results. The data (not shown) were examined for systematic trends, and none were found.

The validity of this or any other data analysis methodology depends ultimately on the quality of the experimental data. Many factors can affect this quality, such as unequal excitation of different mass ions when using chirp or "impulse" excitation [31], $z$-axis ejection of ions [32], and peak coalescence [33] (where ions of high abundance can completely suppress signals from nearby ions of low abundance).

### *Relative Ion Abundance Measurements*

The considerations for magnitude ratio measurements are analogous to those for absolute magnitudes. One important concern is the accuracy of ratios for widely spaced peaks compared to those in a narrow mass-to-charge ratio range. To consider data in a narrow mass-to-charge ratio range, magnitude ratios for the isotopes of $Pb^{+}$, and likewise for the isotopes of $Pb^{+2}$, were calculated using peak heights. To mimic a wide mass-to-charge ratio range, $Pb^{+2}/Pb^{+}$ magnitude ratios were calculated for each isotope. Ratios of peaks in the narrow mass-to-charge ratio range were about 5% more accurate than ratios of peaks in the wide mass range. The overlap of the side lobes is different for the two sets of peaks, which could contribute to the poorer performance for the wide mass-to-charge ratio range.

### *Testing of Methodology Using FTICR Mass Spectra of Xenon Isotopes*

The quantitation methods discussed above, determined from the analysis of simulated data, were tested using actual FTICR mass spectra of xenon isotopes [34]. The data were obtained with an instrument composed of a laboratory-built vacuum system and prototype 2-tesla superconducting magnet [35], and an IonSpec (IonSpec, Irvine, CA) data station.

The nine naturally occurring isotopes of xenon and their abundances are $^{124}$Xe (0.10%), $^{126}$Xe(0.09%), $^{128}$Xe(1.91%), $^{129}$Xe(26.4%), $^{130}$Xe(4.1%), $^{131}$Xe(21.2%), $^{132}$Xe(26.9%), $^{134}$Xe(10.4%), and $^{136}$Xe(8.9%). Only six of these nine isotopes were investigated in this study. The $^{124}$Xe and $^{126}$Xe peaks were not discernible above the noise in the spectra used for quantitation, and the $^{130}$Xe peak exhibited a split appearance, perhaps due to poor homogeneity of the prototype 2-tesla magnet. Thirty spectra were analyzed, with each spectrum obtained by summing 100 transient response signals prior to Fourier transformation. The 30 spectra were background corrected, apodized using the Hanning apodization function (appropriate given the dynamic range of the peaks involved), modified by various degrees of zero filling (0–3), and transformed.

The 30 spectra were divided into three groups of 10, and the average peak heights and average areas for each set of 10 were evaluated. The first set was used as a quantitation standard to remove the effects of uneven excitation in the heterodyne detection mode. A correction factor was obtained by dividing the true abundance by the respective measured peak abundance, determined using either peak height or area, depending on the subsequent analysis. Peak heights and areas from the second and third sets of measurements were treated as "unknowns" and multiplied by the appropriate correction factor before further data analysis. This approach is similar to the use of relative sensitivity factors in various types of mass spectrometry, including glow-discharge mass spectrometry [36]. Percent errors were then obtained for each "unknown" peak as compared to the natural abundance, and the absolute values of these errors were averaged. This treatment produced data comparable to the simulated data used earlier in this article.

Figure 5 is a bar graph of the APE's for the five peak height determination methods with various orders of zero filling for the two "unknown" xenon isotope spectra. The data are very similar to those in Figure 3. With no zero filling, both the parabolic and Comisarow interpolation methods provide much lower APE's than the Lorentzian, magnitude-Lorentzian, and apex methods. As shown earlier, with increasing orders of zero filling, the error decreases, but the improvements are meager after the first zero filling. In the case of these "real" data, as opposed to the simulated data discussed earlier, parabolic interpolation gives slightly better results than Comisarow interpolation. This may be attributed to slight variations in peak shapes due to poor homogeneity of the prototype magnet.

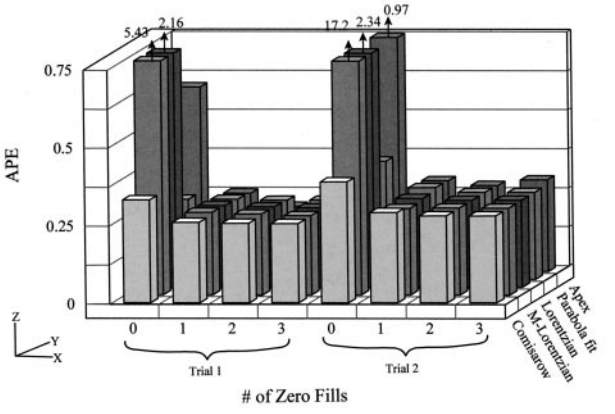


**Figure 5.** Bar graph showing the APE (eq 11) for xenon spectra using peak height as a method for quantitation of ion abundances for various fitting functions and orders of zero filling. The arrows on some bars indicate that they are offscale and have the value above the arrow.

The results using actual mass spectra suggest that, with no zero filling, either the parabolic or Comisarow methods may be used. With one order of zero filling, all interpolation schemes give approximately the same results. Considering the results of the studies of both the simulated and real data, use of the Comisarow interpolated peak height with one order of zero filling is a good general approach to determining ion abundances from peak height measurements.

Figure 6 is a bar graph analogous to Figure 4 for the two "unknown" mass spectra. The results are similar to those obtained for the simulated datasets, with the integrated Comisarow method being superior in all situations. Thus, the data from actual mass spectra corroborate the recommendation based on simulated data that the integrated Comisarow method should be used for quantitating ion abundances by peak area

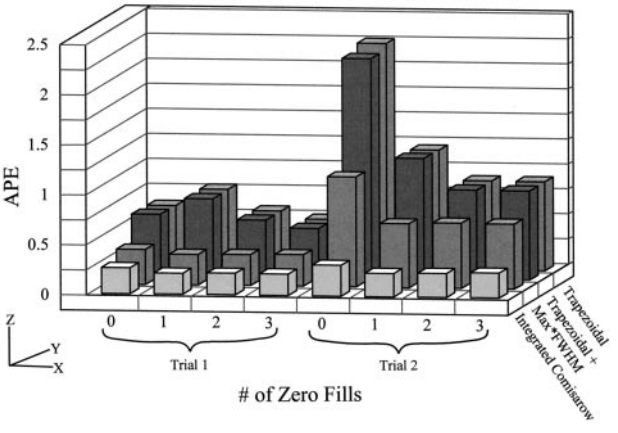


**Figure 6.** Bar graph showing the APE (eq 11) for xenon spectra using peak area as a method for quantitation of ion abundances for various fitting functions, noise levels, and orders of zero filling.

measurements. Figures 5 and 6 show that with one order of zero filling and the Comisarow evaluation method, the APE's for peak height measurements are about equal to the APE's for peak areas. Thus, quantitation by either type of measurement should produce acceptable results.

## Conclusions

Peaks in a series of 384 simulated FTICR-MS spectra, chosen to mimic a range of "real-world" situations, were analyzed to determine optimum conditions for quantitation of peak magnitudes. Combinations of three noise levels, four dataset sizes, four levels of zero filling, and four apodization methods were utilized, and peak magnitudes were evaluated by both peak height (five methods) and peak area (four methods) measurements.

Based on the results, several suggestions for the best quantitation method can be made. Starting with the transient signal, either the Hanning, three-term Blackman-Harris, or Kaiser-Bessel apodization function should be used, depending on the relative magnitudes of the peaks to be analyzed. The time-domain transient should then be zero filled until there are between 10 and 15 points spanning each peak of interest. For peak height measurements, the Comisarow interpolation method, which utilizes a fitting function specific to the apodization type [21], should be used. If peak area determinations are desired, the integrated Comisarow method, described in this paper, produces the most accurate results. This recommended methodology was confirmed when applied to actual FTICR mass spectra of xenon isotopes.

## Acknowledgment

This research was supported in part by the Office of Naval Research.

## References

1. Cassady, C. J.; Carr, S. R. *J. Mass Spectrom.* **1996,** *31*, 247–254.
2. Wu, Q. Y.; Vanorden, S.; Cheng, X. H.; Bakhtiar, R.; Smith, R. D. *Anal. Chem.* **1995,** *67*, 2498–2509.
3. O'Connor, P. B.; Little, D. P.; McLafferty, F. W. *Anal. Chem.* **1996,** *68*, 542–545.
4. Speir, J. P.; Amster, I. J. *J. Am. Soc. Mass Spectrom.* **1995,** *6*, 1069–1078.
5. Sannes, K. A.; Brauman, J. I. *J. Phys. Chem.* **1996,** *100*, 7471–7479.
6. Rodgers, M. T.; Campbell, S.; Marzluff, E. M.; Beauchamp, J. L. *Int. J. Mass Spectrom. Ion Processes* **1995,** *148*, 1–23.
7. Cody, R. B.; Freiser, B. S. *Anal. Chem.* **1982,** *54*, 1431–1433.
8. White, R. L.; Onyiriuka, E. C.; Wilkins, C. L. *Anal. Chem.* **1983,** *55*, 339.
9. Stockigt, D.; Schwarz, J.; Schwarz, H. *J. Phys. Chem.* **1996,** *100*, 8786–8790.
10. Aarstol, M.; Comisarow, M. B. *Int. J. Mass Spectrom. Ion Processes* **1987,** *76*, 287–297.
11. Lee, J. P.; Comisarow, M. B. *Appl. Spectrosc.* **1987,** *41*, 93–98.
12. Lee, J. L.; Chow, K. H.; Comisarow, M. B. *Anal. Chem.* **1988,** *60*, 2212–2218.
13. Brenna, J. T.; Creasy, W. R. *Int. J. Mass Spectrom. Ion Processes* **1989,** *90*, 151–166.
14. Mitchell, D. W.; DeLong, S. E. *Int. J. Mass Spectrom. Ion Processes* **1990,** *96*, 1–16.
15. Lee, J. L.; Comisarow, M. B. *Appl. Spectrosc.* **1989,** *43*, 599–604.
16. Chen, L.; Cottrell, C. E.; Marshall, A. G. *Chemometr. Intelligent Lab. Syst.* **1986,** *1*, 51–58.
17. Comisarow, M. B.; Melka, J. D. *Anal. Chem.* **1979,** *51*, 2198–2207.
18. Liang, Z.; Marshall, A. G. *Anal. Chem.* **1990,** *62*, 70–75.
19. Serreqi, A.; Comisarow, M. B. *Appl. Spectrosc.* **1987,** *41*, 288–295.
20. Filler, A. S. *J. Opt. Soc. Am.* **1964,** *54*, 762–767.
21. Keefe, C. D.; Comisarow, M. B. *Appl. Spectrosc.* **1990,** *44*, 600–613.
22. Watson, C. H.; Goodner, K. L.; Eyler, J. R. *44th ASMS Conference on Mass Spectrometry and Allied Topics*; Portland, OR, 1996; p 1191.
23. *CRC Handbook of Chemistry and Physics, 71st ed.*; Lide, D. R., Ed.; CRC: Boca Raton, FL, 1990; pp A34–A35.
24. Skoog, D. A.; Leary, J. J. *Principles of Instrumental Analysis*; Harcourt Brace Jovanovich: New York, 1992; pp 53–54.
25. Guan, S.; Li, G. Z.; Marshall, A. G. *Proceedings of the 44th ASMS Conference on Mass Spectrometry and Allied Topics*; Portland, OR, 1996; p 493.
26. Cooley, J. W.; Tukey, J. W. *Math. Comput.* **1965,** *19*, 297.
27. Kolman, B. *Elementary Linear Algebra, 4th Edition*; Macmillan: New York, 1986; p 34.
28. Marshall, A. G.; Guan, S. *Rapid Commun. Mass Spectrom.* **1996,** *10*, 1819–1823.
29. Bartholdi, E.; Ernst, R. R. *J. Magn. Reson.* **1973,** *11*, 9–19.
30. Marshall, A. G. *Anal. Chem.* **1979,** *51*, 1710–1714.
31. McIver, R. T., Jr.; Hunter, R. L.; Baykut, G. *Anal. Chem.* **1989,** *61*, 489–491.
32. Wang, M.; Marshall, A. G. *Anal. Chem.* **1989,** *61*, 1288–1293.
33. Mitchell, D. W.; Smith, R. D. *J. Mass Spectrom.* **1996,** *31*, 771–790.
34. Goodner, K. L. Ph.D. Thesis, University of Florida, 1996; Figure 5.8.
35. Yang, Y.; Linnert, H. V.; Riveros, J. M.; Williams, K. R.; Eyler, J. R. *J. Phys. Chem. A* **1997,** *101*, 2371–2378.
36. Application of relative sensitivity factors in glow discharge–FTICR mass spectrometry was discussed in Barshick, C. M.; Eyler, J. R. *J. Am. Soc. Mass Spectrom.* **1992,** *3*, 122–127.